# Complexity analysis of spatiotemporal pattern of local field potentials from motor cortex.

Narayan Puthanmadam Subramaniyam *Student Member, IEEE*, Jari Hyttine *Member, IEEE*,
Kazutaka Takahashi*, *Senior Member, IEEE*,

***Abstract*— Aggregate signals that reflect activities of a large number of neurons in the cerebral cortex, local field potentials (LFPs) have been observed to mediate gross functional activities of a relatively small volume of the brain tissues. There are several bands of the oscillations frequencies in LFPs have been observed across multiple brain areas. The signature oscillation band of the LFPs in the primary motor cortex (MI) is over $\beta$ range and it has been consistently observed both in human and non-human primates around the time of visual cues and movement onsets. However, its dynamical behavior has not been well characterized. Furthermore, spatiotemporal dynamics of $\beta$ oscillations has been documented based on the phase gradient of $\beta$ oscillations, but not in terms of the inherent dynamics of the oscillations themselves. Here, we used the complexity measure derived from cluster coefficients of a recurrent network and analyzed a wide-band and $\beta$ band of the LFPs in MI recorded from a non-human primate. We show a rather unique temporal profile of the complexity of the dynamical behavior of the oscillation, which are not resembling either the power of the oscillation or the phase locking of $\beta$ oscillations. Furthermore, there appears to show some spattiotemporal patterns over the recorded part of MI. Our new approach may give us more insight as to how local circuitry of the cortex is temporally and spatially organized for its function.**

***Index Terms*— premotor cortex, motor cortex, decoding, variational Bayesian inference, functional connectivity**

## I. Introduction

Cortical rhythms have been extensively studied since early descriptions of oscillations in sensorimotor cortex by Jasper and Penfield [1]. Since In particular, local field potentials (LFPs) and electroencephalograms (EEG) in the $\beta$ frequency range (15-40 Hz) are ubiquitous in the motor cortex of mammals including monkeys and humans across the upper limb area of the primary motor cortex (MI). The dynamics of the $\beta$ oscillation has been grossly characterized, based on a temporal profile of the amplitude of the oscillations, such as event related synchronization (ERS) and event related desynchronization (ERD) [2], [3], and phase locking to the instruction cues [4]. However, the dynamical properties of $\beta$ oscillations have not been well characterized. Recently, it has been reported that phase of $\beta$ oscillations propagated as plane waves along the rostrocaudal axis of the motor cortex during motor preparation and execution, and are believed to subserve cortical information transfer [5]. However, it has not been shown inherent dynamics of LFPs, in particular, $\beta$ oscillations, and their spatiotemporal dynamics.

[5], [6]

## II. Method

### A. Behavior task and data collection

All of the surgical and behavioral procedures were approved by the University of Chicago IACUC and conform to the principles outlines in the Guide for the Care and Use of Laboratory Animals. One monkey was trained to perform a visuomotor task using a two-link exoskeleton manipulandum [**?**]. The monkey was required to move a cursor on a horizontal screen that was aligned to the monkey's hand to the position of a target. When the monkey successfully reached the current target, a new target was displayed at a random location within a workspace while the current target disappeared. The monkey received a juice reward after successfully acquiring five or seven consecutive targets.

We recorded local field potentials (LFPs) from up to 96 channels simultaneously at 1 kHz from MI in the monkey using an Utah microelectrode array (Blackrock Microsystems; 1 mm in length and $400\mu$m inter-electrode spacing) implanted contralateral to the moving arm. We analyzed 1000 consecutive successful trials. The LFPs were bidirectionally lowpass filtered at 200 Hz with a 3rd order Butterworth filter. The partitioned into a series of windows of 150 ms starting from the following time windows istarting $[-100, 50]$ ms in relation to visual cue onset, incremented by 10 ms up to $[200, 350]$ ms.

### B. Recurrence Networks

Given an univariate time series $\{u(i), i = 1, 2, \cdots, N\}$, one can reconstruct the phase space trajectory of the underlying dynamics using the method of delays ref. [7]

$$\mathbf{x}_i = (u(i), u(i+\tau), \cdots, u(i+(m-1)\tau)), \tag{1}$$

where $\mathbf{x}_i \in \mathbb{R}^m$, $\tau$ is the embedding delay determined as the first local minimum of the auto mutual information and $m$ is the embedding dimension which can be determined using the false nearest neighbor (FNN) approach. One can visualize the dynamics of the phase space trajectories using the method of recurrence plots ref. [8]. A Recurrence plot (RP) is a graphical representation of the recurrence matrix, which is a closeness test depicting the times when two states visit roughly the same area in phase space. This closeness can be defined based on Euclidean or Manhattan or maximum norm. A recurrence matrix $\mathbf{R}$ depicting the closeness between the pairs of state vectors can be given as in [9], [10]

$$R_{i,j}(\epsilon) = \Theta(\varepsilon - \|x_i - x_j\|), \tag{2}$$

where $\Theta(\cdot)$ is the Heaviside function, $\|\cdot\|$ is a distance norm, and $\varepsilon$ is the recurrence threshold specifying the maximum spatial distance of neighboring states. The recurrence matrix is a binary, symmetric matrix with an entry of 1 if the distance between two states is less than the recurrence threshold $\varepsilon$, else the entry is 0. The recurrence matrix can be reinterpreted as an adjacency matrix after the following transformation [9], [10],

$$\mathbf{A} = \mathbf{R} - \mathbf{I}, \tag{3}$$

where $\mathbf{I}$ is the identity matrix. The above operation simply eliminates the artificial self-loops. The adjacency matrix $\mathbf{A}$ represents an

N.P. Subramaniyam and J. Hyttine are with (Email: {narayan.ps, jari.hyttinen}@tut.fi,) This work was supported ... .K. Takahashi is with Department of Organismal Biology and Anatomy, University of Chicago, IL 60637 USA. (Email: kazutaka@uchicago.edu)

undirected, unweighted complex network known as the recurrence network ref. [10]. The recurrence network can be characterized using graph theoretical methods to reflect the dynamically invariant properties of the associated dynamical system. In this work, we compute the global clustering coefficient $C$ of the recurrence network. Given a network with $N$ nodes and $V$ vertices, the local clustering coefficient of a node $i$ can be defined as the likelihood that the neighbors of $i$ will also be neighbors of each other. Formally, the local clustering coefficient of a node $i$ can be given as in [11],

$$c(i) = \frac{\sum_{j,r} A_{i,j} A_{j,r} A_{r,i}}{k_i(k_i - 1)}, \tag{4}$$

where $k$ is the degree of a node. The Global clustering coefficient is simply the average of local clustering coefficient computed over all the nodes of a network and is given as,

$$C = \frac{1}{N} \sum_{i \in \mathcal{N}} c(i). \tag{5}$$

In order to perform the analysis described above, we divided the LFP data from all the 96 channels into 8 overlapping windows for each event and computed the recurrence network measure $C$ for each window. In order to find the optimal embedding parameters, we computed the first minimum of the auto mutual information for data from all the channels and found that $\tau$ varied between 2 to 4. Similarly, to determine the embedding dimension, we used the improved FNN approach [12] to avoid spurious effects due to noise and found that the embedding dimension varied between 3 to 5 for all the data. Thus we fixed the embedding delay at 6 and the embedding dimension at 5 (it varied between 3 and 5 as per the modified FNN method) to construct recurrence networks of the same size. Instead of specifying the recurrence threshold $\varepsilon$, we fix the recurrence rate $RR = 0.03$ so that we obtain recurrence networks with approximately the same number of edges so that we can compare the networks obtained from different time windows [13].

## III. Results

### A. Temporal profiles of cluster coefficients

The cluster coefficients

### B. Spatiotemporal profiles of cluster coefficients

As shown in Fig. **??**, most causal interactions were detected for Time Window 2 than other two intervals. These causality networks were obtained from the data set1, and we obtained similar results using data sets 2 and 3 as well. In order to look into the causality network consistency over data sets, we plotted the degrees of all neurons for 3 data sets in Fig. 8. All data sets had similar distributions of degrees and same 'hub' neurons 9 and 15 - neurons with unusually high degree. Interestingly neurons recorded from a same electrode were not interacting with one another, but they were causally influencing on neurons from different electrodes.

## IV. Discussions

## V. Acknowledgement

The authors would like to thank M. Togawa, Y. Yamanishi, and N. Takahashi at NIPS and T. Umeda currently at department of neuroanatomy, Yokohama City University for surgery and training of monkeys.

## References

[1] Herbert Jasper and Wilder Penfield, "Electrocorticograms in man: Effect of voluntary movement upon the electrical activity of the precentral gyrus," *Archiv fr Psychiatrie und Nervenkrankheiten*, vol. 183, no. 1-2, pp. 163–174, 1949.

[2] C Neuper and G Pfurtscheller, "Event-related dynamics of cortical rhythms: frequency-specific features and functional correlates," *International Journal of Psychophysiology*, vol. 43, no. 1, pp. 41 – 58, 2001, Thalamo-Cortical Relationships.

[3] Michael T. Jurkiewicz, William C. Gaetz, Andreea C. Bostan, and Douglas Cheyne, "Post-movement beta rebound is generated in motor cortex: Evidence from neuromagnetic recordings," *NeuroImage*, vol. 32, no. 3, pp. 1281 – 1289, 2006.

[4] A Reimer, P Hubka, A K Engel, and A Kral, "Fast propagating waves within the rodent auditory cortex," *Cereb Cortex*, vol. 21, pp. 166–177, 2011.

[5] Doug Rubino, K A Robbins, and Nicholas G Hatsopoulos, "Propagating waves mediate information transfer in the motor cortex.," *Nature Neuroscience.*, vol. 9, no. 12, pp. 1549–1557, Dec. 2006.

[6] Kazutaka Takahashi, Maryam Saleh, Richard D Penn, and Nicholas Hatsopoulos, "Propagating waves in human motor cortex," *Front Hum Neurosci.*, vol. 5, no. 0, 2011.

[7] Floris Takens, "Detecting strange attractors in turbulence," in *Dynamical systems and turbulence, Warwick 1980*, pp. 366–381. Springer, 1981.

[8] J-P Eckmann, S Oliffson Kamphorst, and David Ruelle, "Recurrence plots of dynamical systems," *EPL (Europhysics Letters)*, vol. 4, no. 9, pp. 973, 1987.

[9] Norbert Marwan, Jonathan F Donges, Yong Zou, Reik V Donner, and Jürgen Kurths, "Complex network approach for recurrence analysis of time series," *Physics Letters A*, vol. 373, no. 46, pp. 4246–4254, 2009.

[10] Reik V Donner, Yong Zou, Jonathan F Donges, Norbert Marwan, and Jürgen Kurths, "Recurrence networksa novel paradigm for nonlinear time series analysis," *New Journal of Physics*, vol. 12, no. 3, pp. 033025, 2010.

[11] Duncan J Watts and Steven H Strogatz, "Collective dynamics of small-worldnetworks," *nature*, vol. 393, no. 6684, pp. 440–442, 1998.

[12] Rainer Hegger and Holger Kantz, "Improved false nearest neighbor method to detect determinism in time series data," *Physical Review E*, vol. 60, no. 4, pp. 4970, 1999.

[13] Reik V Donner, Michael Small, Jonathan F Donges, Norbert Marwan, Yong Zou, Ruoxi Xiang, and Jürgen Kurths, "Recurrence-based time series analysis by means of complex network methods," *International Journal of Bifurcation and Chaos*, vol. 21, no. 04, pp. 1019–1046, 2011.

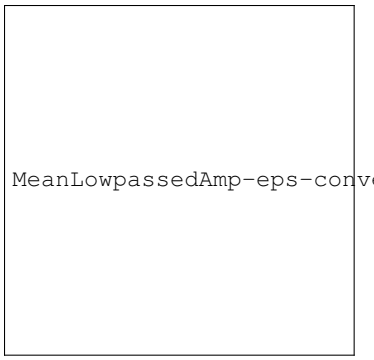


Fig. 1. Temporal profile of amplitude of lowpassed LFPs at 200 Hz around the target appearance which is indicated at 0 ms.

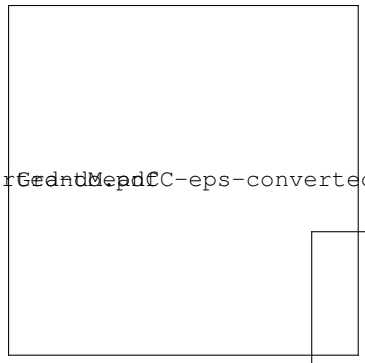


Fig. 2. Temporal profile of cluster coefficients, $C$ for $\beta$ oscillation around the target appearance which is indicated at 0 ms.

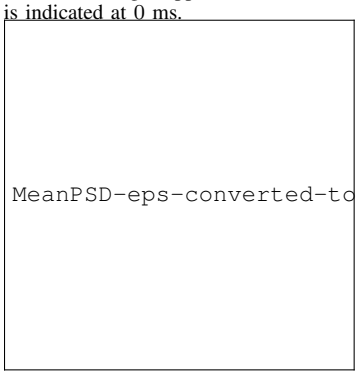


Fig. 3. Averaged power spectrum of LFPs computed over $[-150, 300]$ms around the target appearance for all used events.

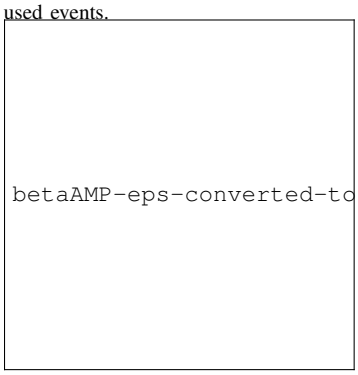


Fig. 4. Temporal profile of amplitude of $\beta$ oscillation around the target appearance which is indicated at 0 ms.

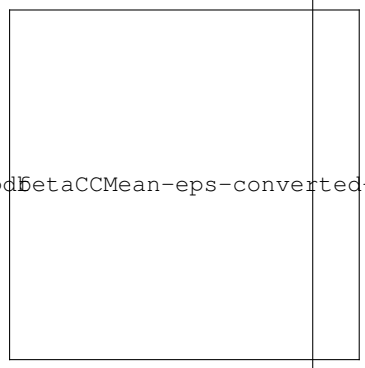


Fig. 5. Temporal profile of cluster coefficients, $C$ for $\beta$ oscillation around the target appearance which is indicated at 0 ms.

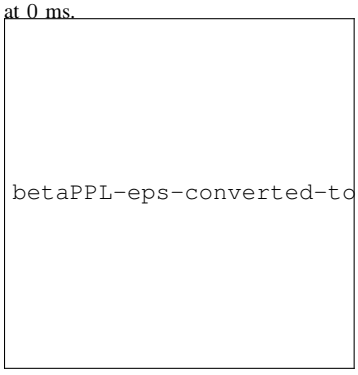


Fig. 6. Temporal profile of percentage of phase locking of $\beta$ oscillation around the target appearance which is indicated at 0 ms.

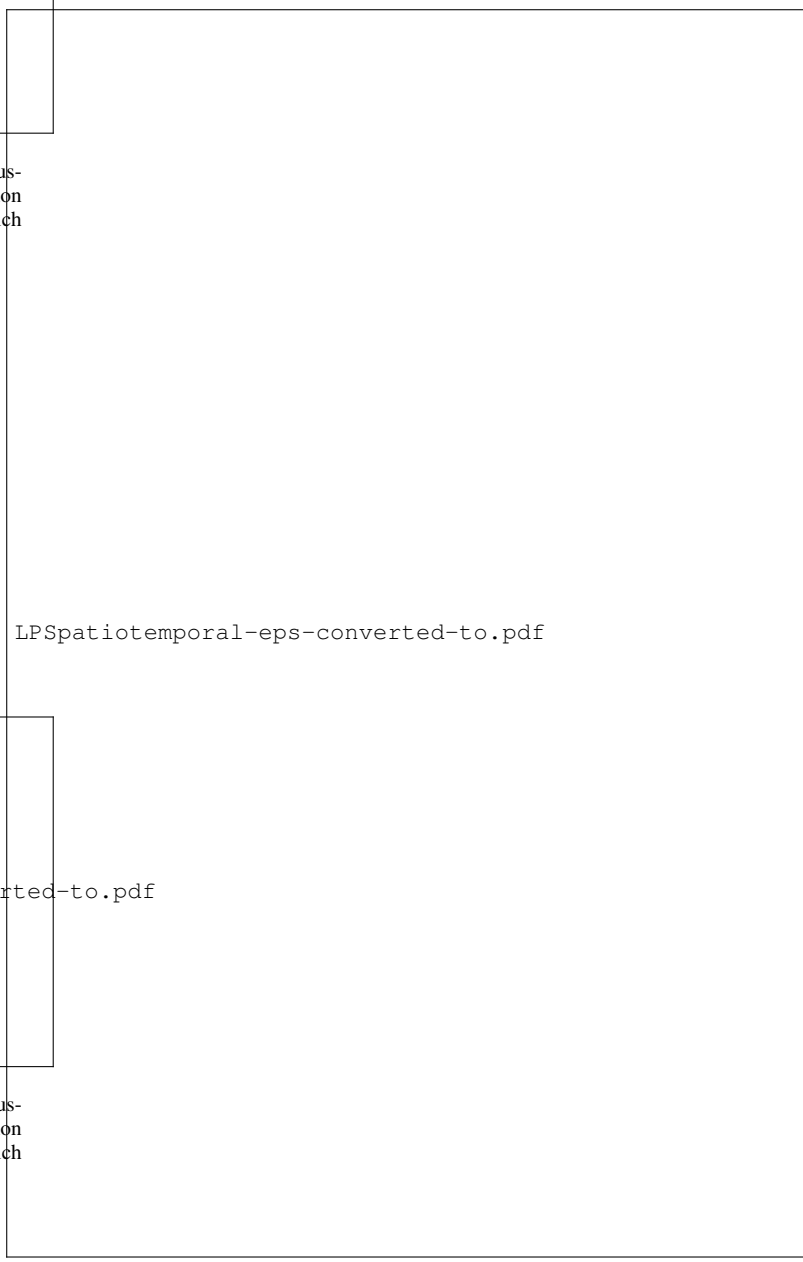


Fig. 7. Cluster coefficients of lowpassed signals of each channels over time around the target appearance mapped to their anatomical locations over the array. R:Rostral, C:Caudal, M:Medial, and L:Lateral.

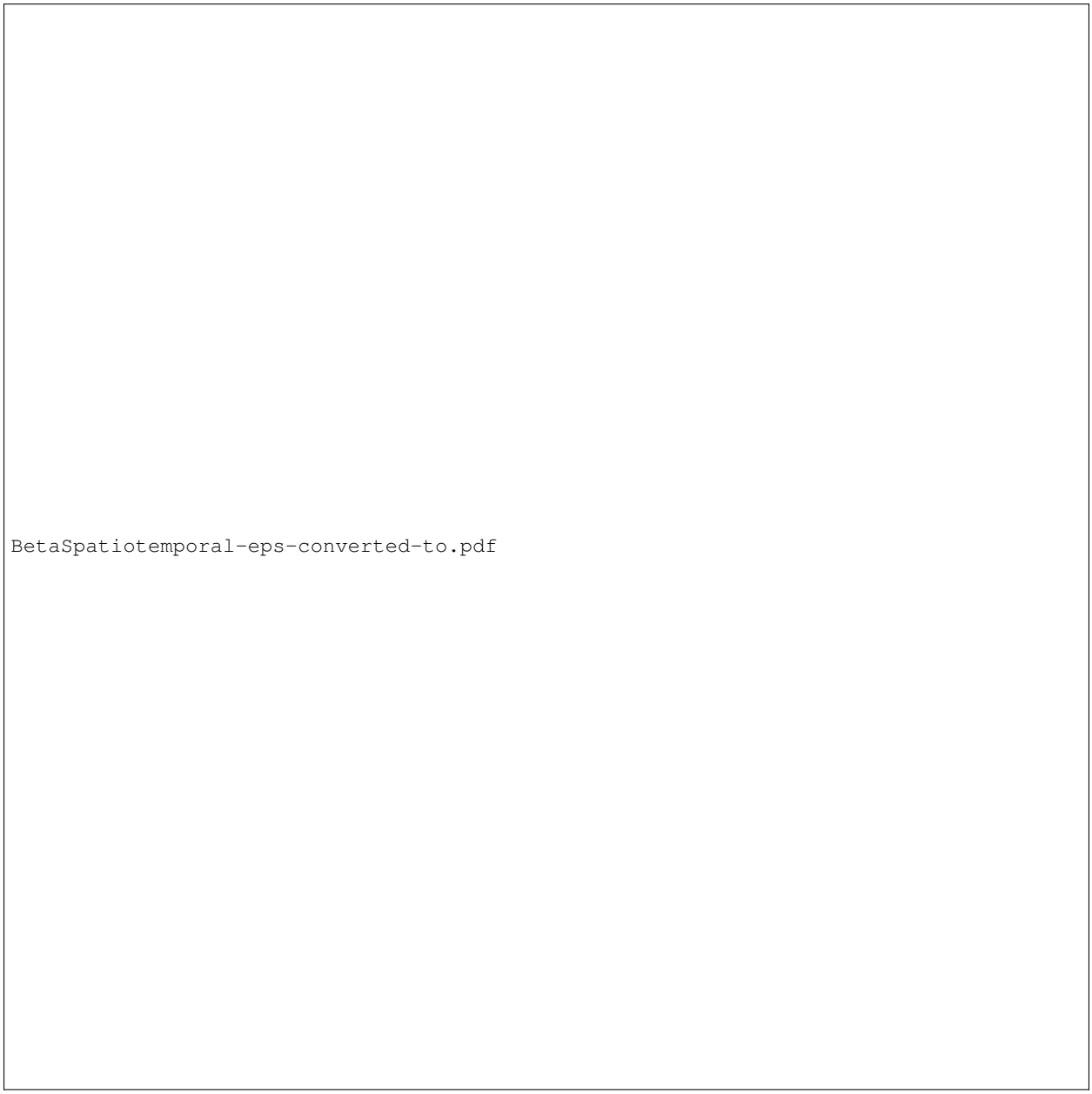


Fig. 8. Same as Fig. 7, but for $\beta$ range of LFPs.